JOURNAL OF COMPUTATIONAL PHYSICS 77, 18–39 (1988)

On the Numerical Dissipation of High Resolution Schemes for Hyperbolic Conservation Laws*

CLAUS-DIETER MUNZ

Institut für Neutronenphysik und Reaktortechnik, Kernforschungszentrum Karlsruhe, Postfach 3640, D-7500 Karlsruhe 1, West Germany

Received July 21, 1986, revised April 3, 1987

In recent years, a number of new shock-capturing finite difference schemes, often called high resolution schemes, have been constructed. This paper presents a comparison of these schemes in terms of their numerical dissipation, which becomes very obvious from numerical results obtained for two initial value problems of a two-dimensional advection equation. We consider TVD schemes, which are constructed to prevent the total variation of the numerical approximations from increasing, as well as UNO schemes which only guarantee that the number of local extrema does not increase. © 1988 Academic Press, Inc.

1. INTRODUCTION

In recent years various new shock-capturing schemes have been developed for the approximation of nonlinear one-dimensional hyperbolic conservation laws (see, e.g., [1, 5, 10, 27]). These schemes, usually called "high resolution schemes," have the following properties: They are at least of second-order accuracy in smooth parts of the flow, they sharply resolve discontinuities without generating spurious oscillations, and in contrast to classical second- or higher order schemes, they do not need artificial viscosity. The main building block of most of these schemes are first-order upwind differencing schemes which incorporate into the numerical solution the direction of nonlinear wave propagation. In this way the upwind schemes guarantee the resolution of the discontinuities without wiggles, but they possess a strong numerical dissipation and spread discontinuities over many grid points. The other part of a high resolution scheme is an antidiffusive mechanism which converts the upwind scheme to better resolution of discontinuities and higher accuracy, while the desirable properties are preserved. There are several approaches to obtain a better resolution. The high resolution schemes using flux limiters add an antidiffusive term to the numerical flux of the upwind scheme. This concept was introduced by Boris and Book [2] and van Leer [17]. Another way was indicated

* This work was supported in part by Deutsche Forschungsgemeinschaft (DFG)—Priority Research: "Finite Approximations in Fluid Mechanics"—while the author was affiliated with Kalsruhe University.

0021-9991/88 $3.00

by the MUSCL scheme of van Leer [16]. Here, the higher order solution is achieved by using in each time step a more accurate representation of the initial distribution and then applying an upwind scheme to these data. Harten [10] in his approach applied the upwind scheme to a conservation law with a modified flux. A fourth way, not based on upwind biased differences, was proposed by Davis [8]. As there may be different upwind schemes and on account of these different approaches, there are a great number of high resolution schemes.

In this paper we will compare various high resolution schemes by numerical results for initial value problems for the simplest two-dimensional conservation law, that of a two-dimensional linear advection equation. The one-dimensional schemes are extended to two dimensions by operator splitting which works very well for practical calculations (see, e.g., [7, 28]). Because the numerical smearing of contact discontinuities or linear discontinuities may increase with time—contrary to shock waves—the capturing of these discontinuities is very important. Performing long time calculation differences between various schemes becomes very obvious. As in the case of linearity, different approaches obtaining high resolution lead to the same schemes and all upwind schemes agree with the Courant–Isaacson–Rees scheme [6]; the great diversity of high resolution schemes is rather reduced, and a comparison is possible. Our results will show mainly the efficiency and the properties of the antidiffusive terms used in the different schemes. They will give insight into the shock and contact discontinuity capturing capability of the schemes for nonlinear problems. We will not consider the artificial compression method developed by Harten [11]. As a corrective step Harten added artificial compression to a first-order upwind scheme to compress smeared discontinuities and he obtained a first-order accurate scheme with a very good resolution of discontinuities. In this paper we are interested in explicit second-order accurate schemes which combine the good approximation of discontinuities with a good approximation of smooth parts of the solutions as needed for most of the practial calculations. The results for our test problems measure the artificial compression which is inherent in the second-order high resolution schemes. We note that the artificial compression may also be added to second-order schemes near a discontinuity as a separate step. But, because second-order accuracy limits the amount which can be added, the artificial compression of first-order accuracy may lead to a narrower transition zone of a discontinuity. Our results will show that high resolution schemes with a strong antidiffusive mechanism may be over-compressive in the sense that every monotone transition is compressed into a discontinuity. For nonlinear problems this property may introduce non-physical rarefaction shocks into the numerical solution (see, e.g., [18, 27]). The outcome of our calculations can directly be used for all schemes for the equations of compressible gas dynamics constructed via Roe's [23] or Huang's [13] extension to systems.

This paper is divided into four sections. In Section 2 we will describe the test problems and the discretization parameters used in our numerical calculations. In Section 3 the construction of high resolution schemes will be briefly reviewed and the different schemes will be listed together with their numerical results. Section 4

contains our conclusions and remarks concerning the extension to the equations of compressible gas dynamics.

2. Numerical Test Problems and Discretization Parameters

We will compare the numerical dissipation of explicit high resolution schemes by numerical results for the two-dimensional advection equation

$$u_t + (\alpha(y)u)_x + (\beta(x)u)_y = 0 \tag{1}$$

with

$$\alpha(y) = -(y - y_0)\omega, \qquad \beta(x) = (x - x_0)\omega. \tag{2}$$

The exact solution of (1), (2) consists in the rotation of the initial values round (x_0, y_0) with the angular velocity ω. We will present two series of calculations. As initial values we choose a cut-out cylinder and a cone. These problems seem to be well suited to benchmark the numerical dissipation of the schemes. The numerical results of the cut-out cylinder clearly show the damping of contact discontinuities, while the cone illustrates the preservation of the shape of the solution, especially that of local extrema. Both problems visualize maintenance of the symmetry by the difference schemes. The "rotating cone problem" has been used to test numerical schemes for linear advection equations often (see, e.g., [25]), while the cut-out cylinder was proposed by Zalesak [30]. He used it to demonstrate the shock-capturing capability of his scheme.

We choose the angular velocity ω to be 0.1 and $x_0 = 50$, $y_0 = 50$. The region of computation was $[0, 100] \times [0, 100]$. The numerical calculations were done on a fixed uniform grid with 100 grid points in each direction. At time $t = 20\pi$ the initial values have carried out one full rotation and returned to their initial position. The approximations of the initial values on our grid are shown in Figs. 1, 2. The cone has a base radius of 15 and a maximum value of 4 at the point (75, 50). The cut-out cylinder has the same base radius, the same maximum value and the same position. We performed long time calculations until $t = 120\pi$ which corresponds to six full rotations of the initial values. For the numerical approximations we used 3768 time steps. The numerical results are plotted after one and six full rotations. All calculations have been done on a Siemens 7881 computer using a four byte floating point arithmetic.

3. High Resolution Schemes

We shall consider numerical approximations to a one-dimensional scalar conservation law. For our calculations the one-dimensional schemes were extended to two dimensions by operator splitting, also called the method of fractional steps ([7]).

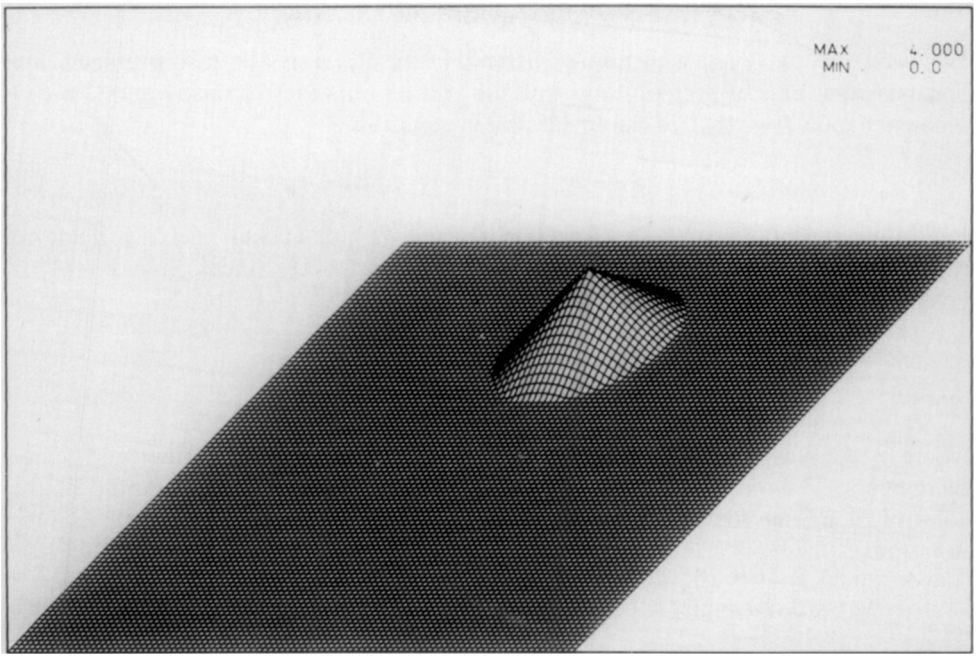

FIG. 1. Initial values and exact solution after each full rotation—cone.

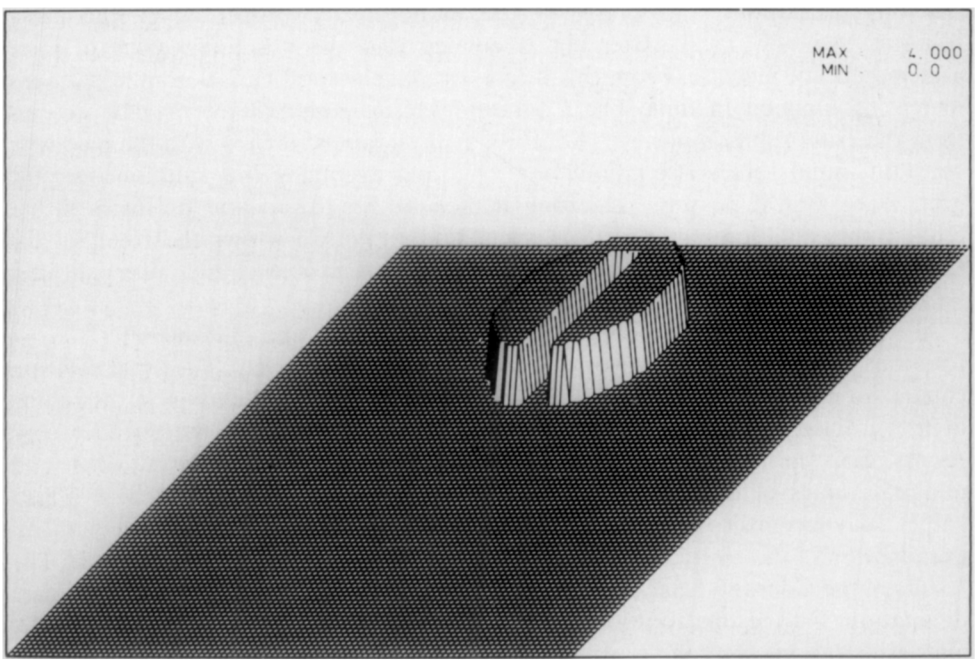

FIG. 2. Initial values and exact solution after each full rotation—cut-out cylinder.

We used the two-cycle splitting of Strang [26]. Because our test problems are linear and for ease of presentation, we shall restrict ourselves to the simplest case of a conservation law, that of the linear scalar equation

$$u_t + cu_x = 0, \qquad c = \text{const.} \tag{3}$$

Regarding the nonlinear case some remarks will be added and reference made to the literature. A first-order explicit upwind scheme for the linear equation (3) is given by the Courant–Isaacson–Rees [6] scheme

$$u_i^{n+1} = u_i^n - \lambda c \begin{cases} u_i^n - u_{i-1}^n & \text{for} \quad c > 0, \\ u_{i+1}^n - u_i^n & \text{for} \quad c < 0, \end{cases} \tag{4}$$

where λ denotes the mesh ratio $\lambda = \Delta t/\Delta x$, Δt and Δx are the time and space increments. The value u_i^n denotes an approximation of the average value of the solution u in the ith grid zone at time $t_n = n\,\Delta t$. Throughout we shall use the notations

$$x_i = i\,\Delta x, \quad x_{i+1/2} = \tfrac{1}{2}(x_i + x_{i+1}), \quad t_n = n\,\Delta t, \quad I_i = [x_{i-1/2}, x_{i+1/2}] \tag{5}$$

with $i \in \mathbb{Z}$, $n \in \mathbb{N}$.

The Courant–Isaacson–Rees scheme is stable under the usual restriction on the mesh ration $\lambda c \leqq 1$, called CFL-condition. It captures discontinuities with no spurious oscillations and preserves the monotonicity properties of the exact solution: No new local extremum is created and the absolute values of local extrema do not increase. From this it follows that the total variation in x is a non-increasing function in time. The Courant–Isaacson–Rees scheme may be derived from the exact solution $u(x, t_{n+1})$ of the Cauchy problem for (3) with the piecewise constant initial values $v(x, t_n) = u_i^n$ for $x \in I_i$ and averaging this solution over the grid zones. But it possesses a strong numerical dissipation and produces rather crude approximations for practical calculations. Figure 3 shows the result of the Courant–Isaacson–Rees scheme applied to both test problems after one and after six full rotations.

All figures show the numerical results obtained after one full and after six full rotations corresponding to 628 and 3768 time steps, respectively. The exact solution equals the initial data (see Figs. 1, 2). Each figure shows on the left side the results of the problem with the cone and on the right side that with the cylinder. The results after one rotation are entered at the top. For every plot the maximal and minimal values of the numerical solution are written at the right corner. These values may be misleading if used alone, but when they are combined with an examination of the plotted numerical solution a valid comparison can be made. The results of the Courant–Isaacson–Rees scheme in Fig. 3 indicate the strong numerical dissipation. During one rotation the peak of the cone decreases from 4.0 to 1.202, after six rotations the cone is almost vanished. The results are quite similar for the cylinder; after one rotation the exact solution is no longer anticipated.

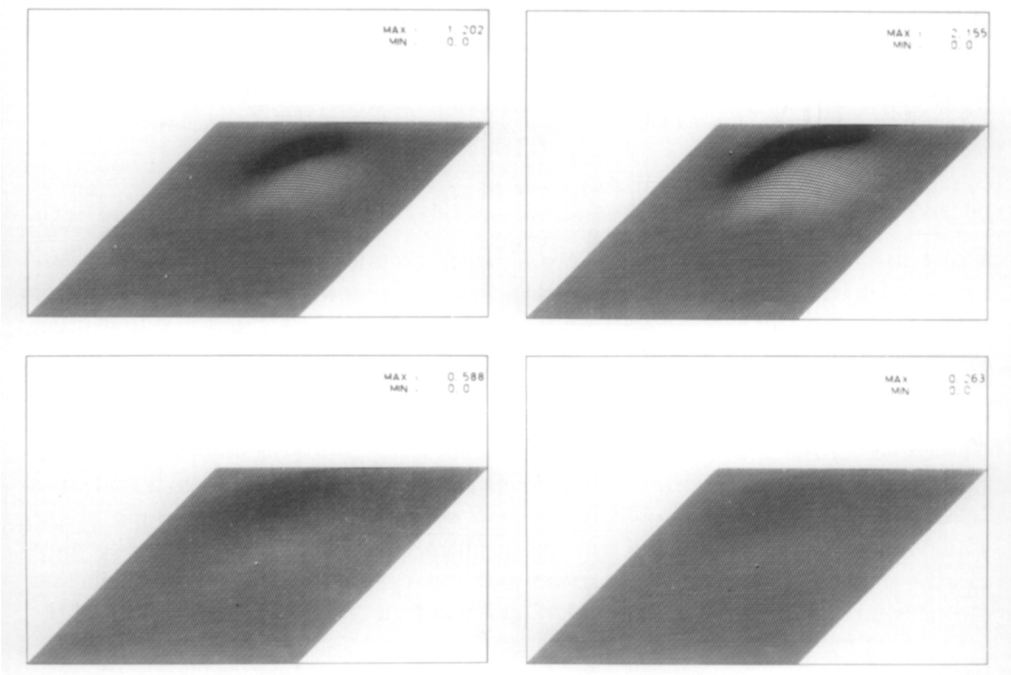

FIG. 3. Courant–Isaacson–Rees scheme.

One way to get better resolution and second-order accuracy is suggested by van Leer's MUSCL approach [16]. Instead of piecewise constant data van Leer considered the piecewise linear data

$$v(x, t_n) = u_i^n + \frac{x - x_i}{2} s_i^n \qquad \text{for} \quad x \in I_i. \tag{6}$$

Next the exact solution of the Cauchy problem for (3) with these initial data is calculated and averaged over the grid zones. In the case $c > 0$ the resulting scheme is

$$u_i^{n+1} = u_i^n - \lambda c(u_i^n - u_{i-1}^n) - \frac{\lambda c}{2}(1 - \lambda c)(\Delta x s_i^n - \Delta x s_{i-1}^n). \tag{7}$$

Starting from the integral average u_i^n of the approximation in I_i at time t_n, the first step in the MUSCL approach is a reconstruction of the solution by a piecewise linear function. Then the upwind method is applied to these data. A necessary condition for this algorithm being of second-order accuracy, both in space and time, is that the slopes are locally weighted averages of right- and left-hand differences

$$s_i^n = u_x(x_i, t_n) + O(\Delta x). \tag{8}$$

For nonlinear problems the exact solution for the Cauchy problem with respect to the initial data (6) in general cannot be determined and is replaced by an approximative one. The piecewise linear distribution (6) defines boundary values in each grid zone

$$u_{i\pm}^n = u_i^n \pm \frac{\Delta x}{2} s_i^n. \tag{9}$$

Using a midpoint rule to obtain second-order accuracy in time these values are advanced by half a time-step and then a first-order upwind scheme is applied to these data (see [15, 16, 5]). By this concept it is easy to convert a low order upwind scheme to higher order accuracy.

If the slopes are selected as right-hand difference quotients, the scheme (7) is identical to the Lax–Wendroff scheme [14] which is based on central differencing. The choice of the left-hand difference quotients leads to the second-order upwind-differencing scheme of Warming and Beam (see [27]). It is well known that both schemes generate spurious oscillations near strong gradients. The results of the Lax–Wendroff scheme for our two test problems are shown in Fig. 4. The plots clearly show wiggles behind the cone and the cylinder. The wiggles which are stronger for the discontinuous initial values also lead to a displaced position of the

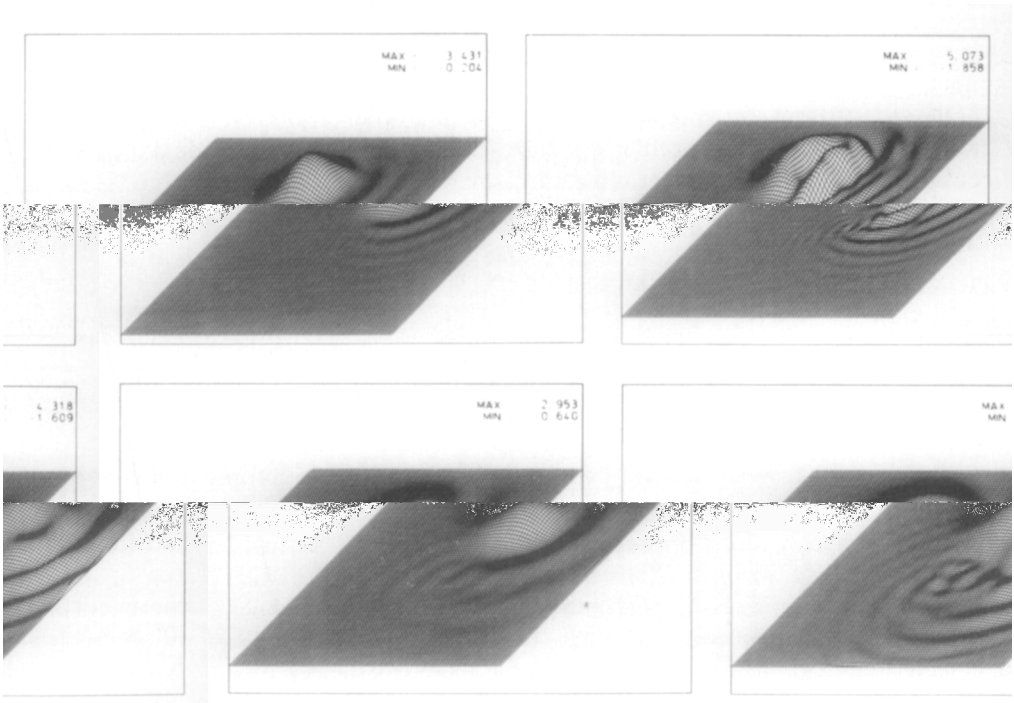

FIG. 4. Lax–Wendroff scheme.

[illegible] the oscillations are somewhat smaller and in front of the cone and cylinder.

The exact solution of (3), (6) and their averaging over the grid zones do neither introduce new local extrema nor accentuate the old ones. Hence the problem to obtain a non-oscillatory algorithm is essentially reduced to find an appropriate monotonicity preserving piecewise linear description of the solution. A whole class of appropriate slopes is given by

$$s_k(a_i, b_i) = \operatorname{sign}(a_i) \max\{|\operatorname{minmod}(ka_i, b_i)|, |\operatorname{minmod}(a_i, kb_i)|\} \quad \text{for} \quad 1 \leqq k \leqq 2 \tag{10}$$

where a_i, b_i denotes the right- and left-hand differences

$$a_i = \frac{u_{i+1} - u_i}{\Delta x}, \qquad b_i = \frac{u_i - u_{i-1}}{\Delta x} \tag{11}$$

and the minmod-function (see [24]) is defined by

$$\operatorname{minmod}(a, b) = \begin{cases} a & \text{for} \quad |a| \leqq |b|, \; ab > 0 \\ b & \text{for} \quad |a| > |b|, \; ab > 0 \\ 0 & \text{for} \quad ab \leqq 0. \end{cases} \tag{12}$$

We drop here and in the following expressions the superscript "n" whenever no misunderstanding will occur. Schemes based on this calculation of the slopes satisfy (8) in smooth parts and preserve the monotonicity properties of the exact solution. The total variation of the approximations do not increase with time; this is called the TVD-property (total variation diminishing) after Harten [9]. Within a semi-discrete approximation (method of lines) Osher [19] gave some criteria for a MUSCL-type scheme to be second-order and TVD. These can be extended to the fully discrete case in a straightforward manner (see [18]). Osher also proved in [19] the convergence of the approximations if the step sizes tend to zero. Although a TVD-scheme can be made second-order accurate in the sense of global error in L^1-norm, it necessarily degenerates at local extrema to first-order accuracy in the sense of local truncation error (see [21]). The slope s of a TVD-scheme will vanish at these points. Consequently local extrema of the numerical solution are damped more strongly which is usually called the "clipping phenomenon." In contrast to the classical second-order schemes as the Lax–Wendroff or Warming and Beam scheme, the high resolution schemes are nonlinear even in the constant coefficient case.

For the linear equation (3) Roe's [22, 24] construction of high resolution schemes agrees with the MUSCL approach. He formulated his schemes in terms of fluctuations, signals, and average functions. He proposed the members of the class (10) $s_1 = \operatorname{minmod}(a_i, b_i)$ and s_2 which he called "superbee." Another concept is that of the schemes using flux limiters which was introduced by Boris and Book [2] and

van Leer [17]. Sweby [27] succeeded in giving a general framework of their construction. If we define the slopes by a switching function or transition function φ,

$$s(a_i, b_i) = a_i \varphi(r_i) \tag{13}$$

depending on the quotient of successive gradients $r_i = b_i/a_i$, then the MUSCL-type scheme equals the Sweby's scheme [27] using the flux limiter φ. Hence, all flux limiters reformulated and reviewed by Sweby [27] may be used to define appropriate slopes via the relation (13). The class of slopes (10) corresponds to the class of flux limiters proposed by Sweby. From (13) it follows that $s(1, r_i) = \varphi(r_i)$ which facilitates geometric illustration in the (r_i, φ)-plane (see [22, 27]). Criteria for TVD-ness and second-order accuracy in terms of the switching function or flux limiter are given by Sweby [27] and Roe [22]. Figures 5 and 6 show the results of two members of the class (10) associated with the minimum and maximum values of k: s_1 and the superbee s_2. The numerical dissipation of the Courant–Isaacson–Rees scheme is strongly reduced. Excellent results for the rotating cut-out cylinder are produced by the superbee slope. But the results for the cone very clearly show a strong clipping phenomenon, the top of the cone is clipped. After six full rotations the maximum value is still 3.337. Later this maximum hardly decreases (3.332 after 12 full rotations), but the shape slowly tends against a cylinder (no figure). The scheme based on s_1 is not as compressive and the results are more strongly dissipated. After six rotations the groove of the cylinder is vanished, but the results after six rotations are still much better than that of the first-order upwind scheme after one rotation. The clipping is not as conspicuous as that of s_2.

A limiter function which is a continuous function of r_i was proposed by van Leer in [17] (see also [27]). The corresponding slope reads

$$s_{\mathrm{VL}}(a, b) = \frac{|ab| + ab}{a + b}. \tag{14}$$

We drop here and in the following expressions the index "i," too; as in (11) a denotes the right-hand and b the left-hand difference quotient. Another slope, due to van Leer [16], is the "monotonized central difference" algorithm

$$s_{\mathrm{M}}(a, b) = \operatorname{minmod}\left(\frac{a+b}{2}, 2 \operatorname{minmod}(a, b)\right) \tag{15}$$

which was given in the context of the MUSCL-scheme (see also [5]). Figure 7 shows the results of the scheme using (14). The maximal values of the approximations are better than that of the scheme using s_1 (Fig. 5). They are similar to those obtained by the element $k = 1.4$ of class (10), but the clipping of (14) is weaker. The scheme based on the monotonized central difference (15) (Fig. 8) for our both problems produced better results than s_1, s_{VL} which can be seen from the maximum values, but the clipping phenomenon is also visible. The excellent resolution of the discontinuity given by the superbee s_2 is not obtained.

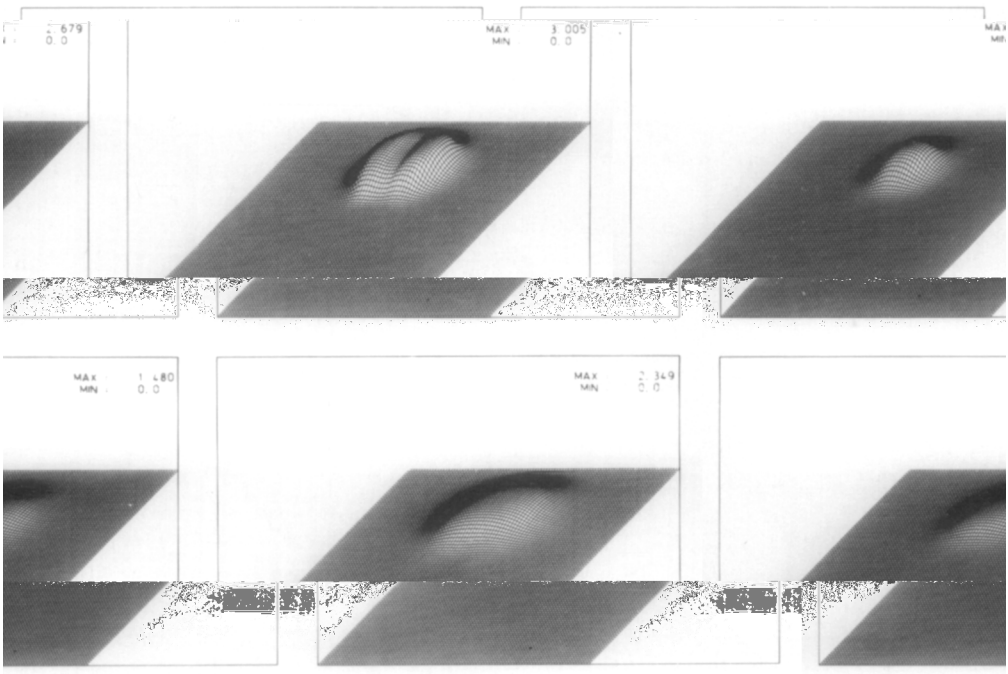

FIG. 5. Scheme based on the slope (10) s_1.

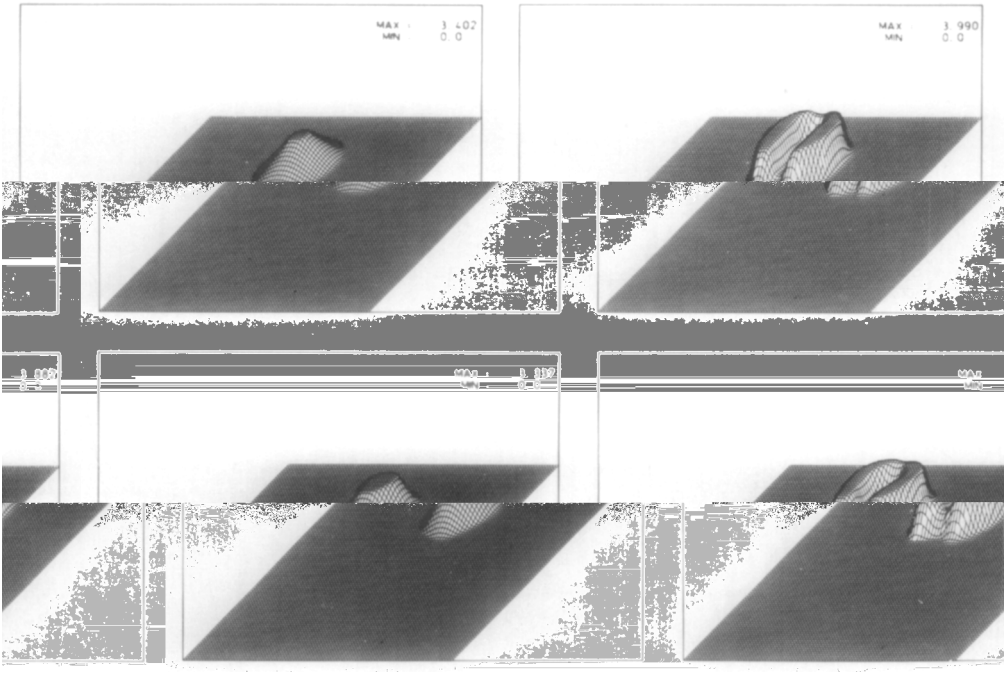

FIG. 6. Scheme based on the superbee slope (10) s_2.

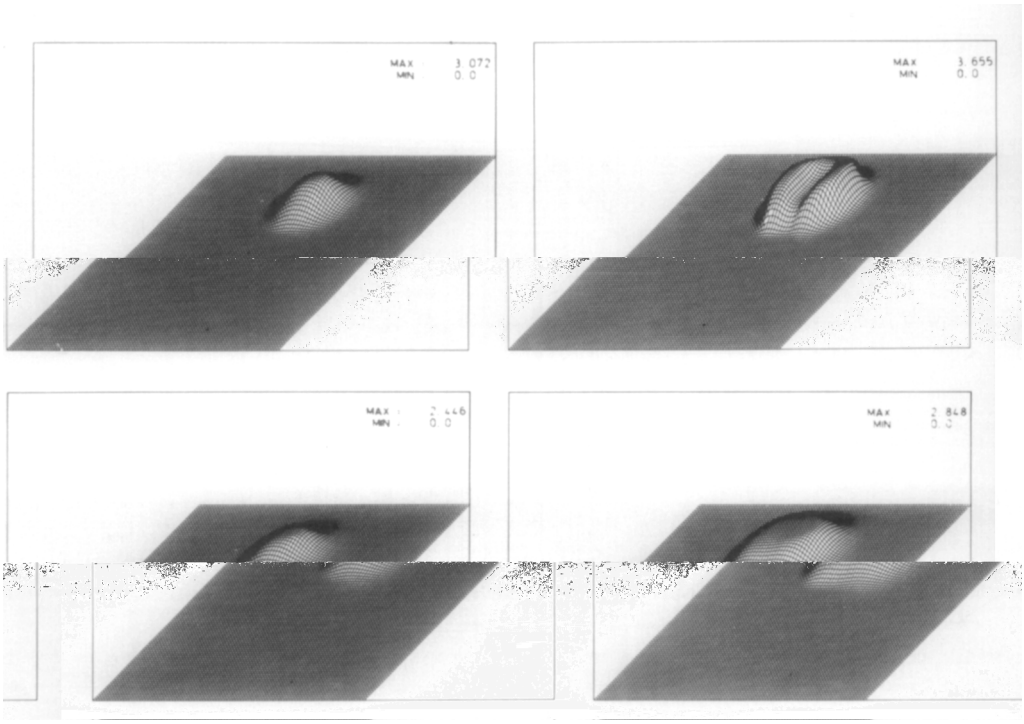

FIG. 7. Scheme based on the slope (14) s_{VL}.

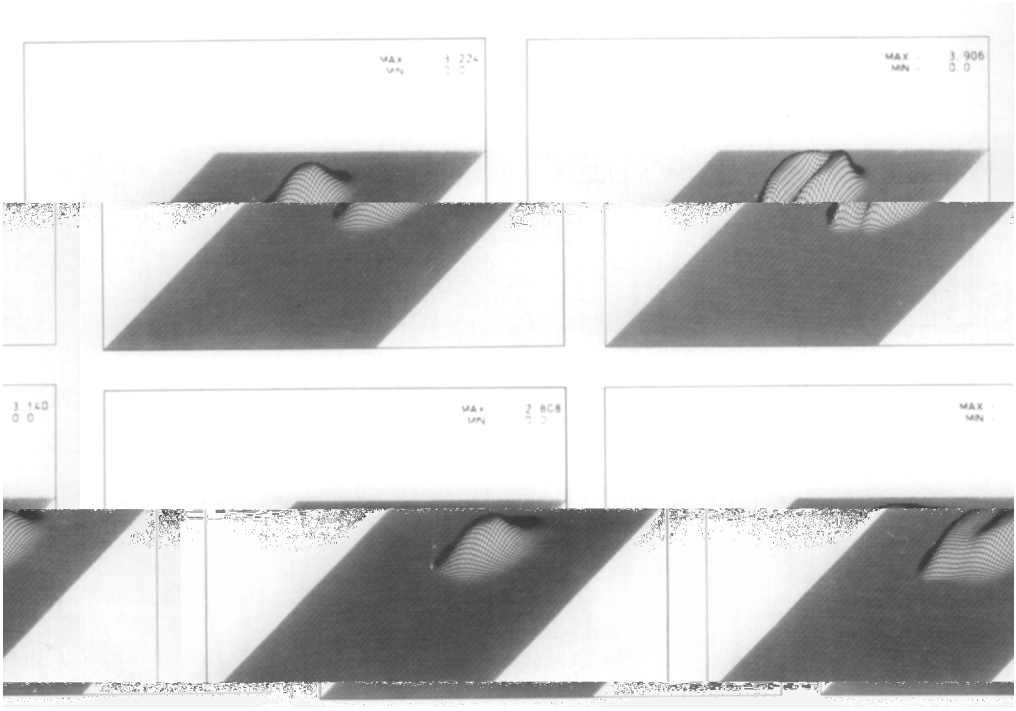

FIG. 8. Scheme based on the slope (15) s_{M}.

All slopes listed above possess the property

$$s(a, b) = s(b, a) \tag{16}$$

which guarantees that forward and backward gradients are treated in the same fashion. We will see that this is an important condition to preserve the symmetry properties of the exact solution. In terms of the transition functions the condition (16) reads $\varphi(r)/r = \varphi(1/r)$ (see [27]). The class of slopes

$$s_{\mathrm{CO},k}(a, b) = \mathrm{minmod}(a, kb) \tag{17}$$

with $1 \leqq k \leqq 2$ which was used by Osher and Chakravarthy [21] does not possess this property unless $k = 1$. The results for the test problems in the most compressive case $k = 2$ are presented in Fig. 9. They show a lack of symmetry. To get a better impression of the symmetry properties we plotted the contour lines of the numerical results for the rotating cone problem in Fig. 17–18.

Another class of high resolution schemes was proposed by Chakravarthy and Osher in [4] in the context of flux limiter, too. This class includes a scheme which is of third-order accuracy in space. It can also be used to define generalized

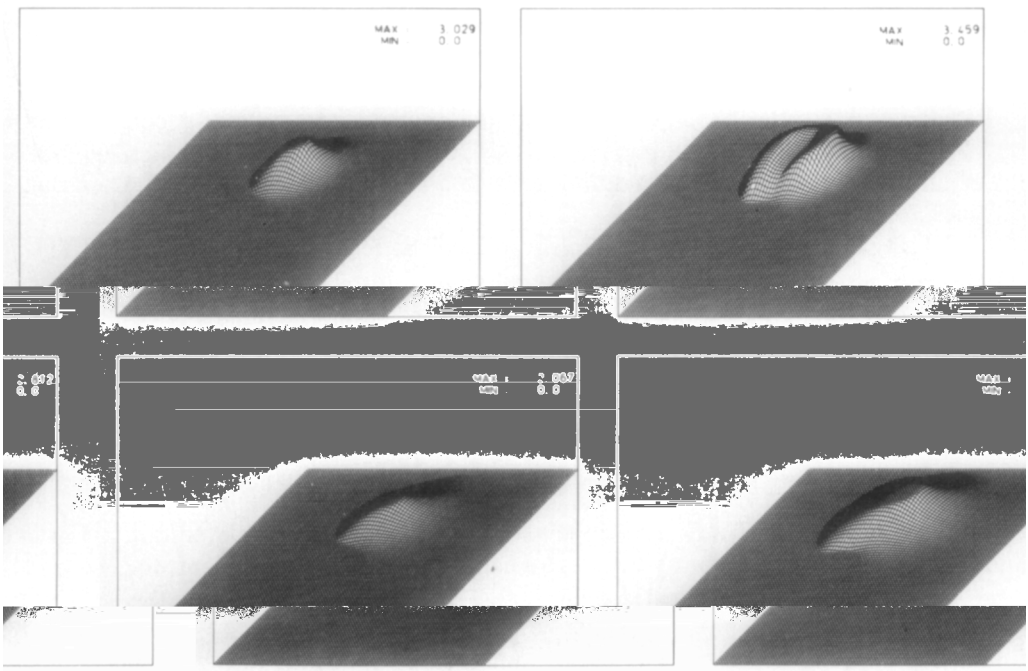

FIG. 9. Scheme based on the slope (17) $s_{\mathrm{CO},2}$.

MUSCL schemes. Instead of (9), the values at the interfaces of the grid zones are defined by

$$u_{i\pm} = u_i \pm \frac{\Delta x}{2}\,\delta_{i\pm}, \tag{18}$$

where the value of $\delta_{i\pm}$ are determined as weighted average values of slopes $\tilde{s}$, $\tilde{\tilde{s}}$

$$\begin{aligned}\delta_{i+} &= \tfrac{1}{2}\left[(1-\theta)\tilde{\tilde{s}}_i + (1+\theta)\tilde{s}_i\right]\\ \delta_{i+} &= \tfrac{1}{2}\left[(1-\theta)\tilde{s}_i + (1+\theta)\tilde{\tilde{s}}_i\right]\end{aligned} \tag{19}$$

with $-1 \leqq \theta \leqq 1$. The slopes $\tilde{s}$, $\tilde{\tilde{s}}$ are defined by

$$\begin{aligned}\tilde{s}_i &= \frac{1}{\Delta x}\,\mathrm{minmod}(a_i, lb_i)\\ \tilde{\tilde{s}}_i &= \frac{1}{\Delta x}\,\mathrm{minmod}(la_i, b_i)\end{aligned} \tag{20}$$

with a_i, b_i from (11). The compression parameter is given within the range $1 \leqq l \leqq (3-\theta)/(1-\theta)$. The boundary values (18) can be written in form (9) only if $l=1$, $-1 \leqq \theta \leqq 1$, with the corresponding slope equal to s_1 or if $\theta = 0$, $1 \leqq l \leqq 3$. In the case $\theta = 0$, $l = 3$ the slope agrees with s_M. Beside these cases the schemes based on (18) do not satisfy a symmetry condition. The value $\theta = \frac{1}{3}$ leads to a scheme which is of third-order accuracy in space. Figures 10–12 show the results of these schemes for $\theta = \frac{1}{3}$, $\frac{1}{2}$, and -1, respectively, and the optimal corresponding compression parameter l. They produce good results as regards the maximum values, but the invalidity of the symmetry condition leads to a non-symmetric shape. The contour lines are plotted in Fig. 19.

All slopes considered above vanish at local extrema. The schemes are TVD-schemes and hence degenerate at local extrema to first-order accuracy in the sense of the local truncation error (see [21]). The stronger damping at these points is clearly seen from our results. To overcome this drawback of TVD-schemes, van Albada *et al.* [1] proposed a slope which does not vanish at these points

$$s_{VA}(a, b) = \frac{(ab + \varepsilon^2)(a+b)}{a^2 + b^2 + 2\varepsilon^2}, \tag{21}$$

where ε^2 is a small value of $O(\Delta x)$. The slope (21) satisfies the symmetry condition (16) and is still TVD in regions away from extrema. Especially in these regions, the slope s_{VA} with $\varepsilon = 0$ is always smaller than s_{VL}. The results achieved with this scheme are shown in Fig. 13. Results similar to that for s_{VL} are obtained but a slight undershoot arose at the base of the figures. The results are quite similar for a wide range of values of ε; we used in our calculations $\varepsilon^2 = 0.008$.

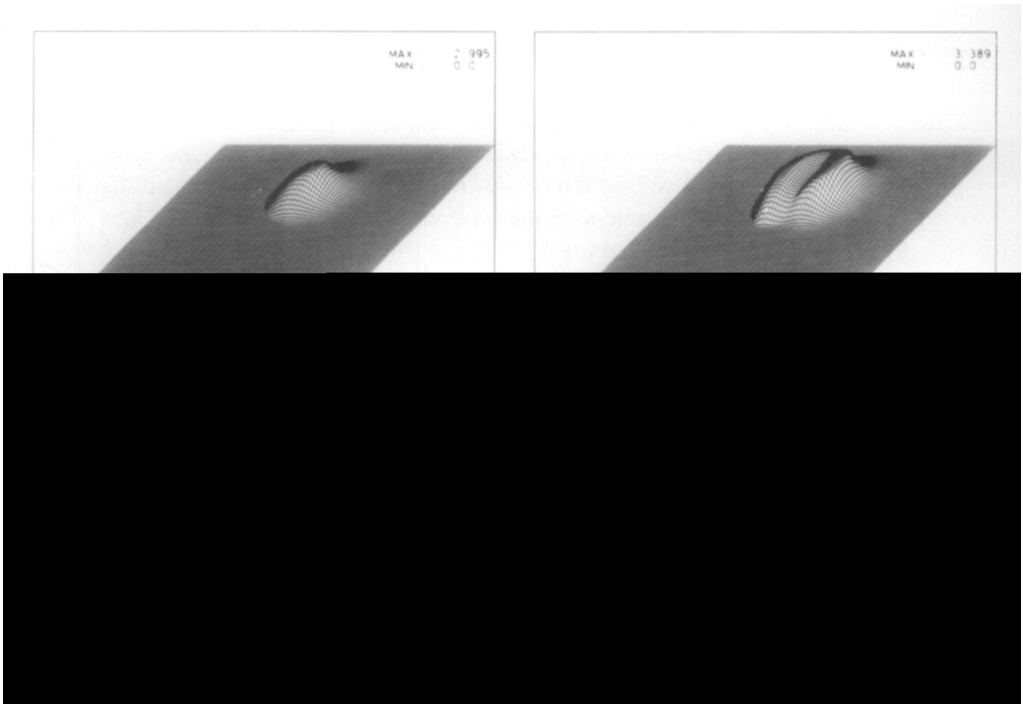

FIG. 10. Scheme based on the slope (18)–(20) with $\theta = \frac{1}{3}$, $l = 4$.

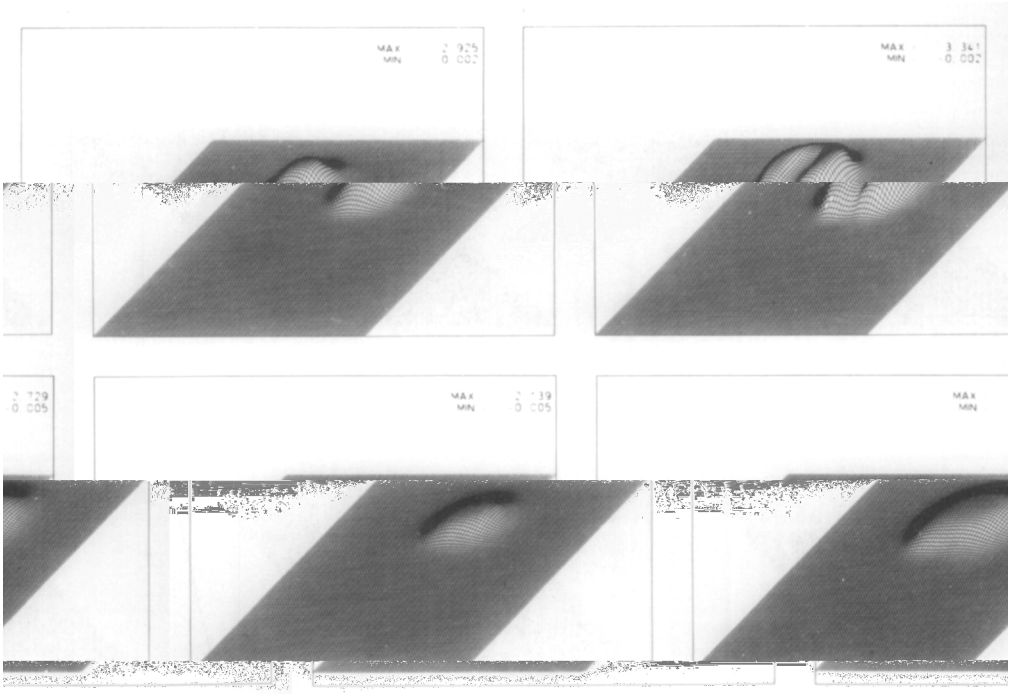

FIG. 11. Scheme based on the slope (18)–(20) with $\theta = \frac{1}{2}$, $l = 5$.

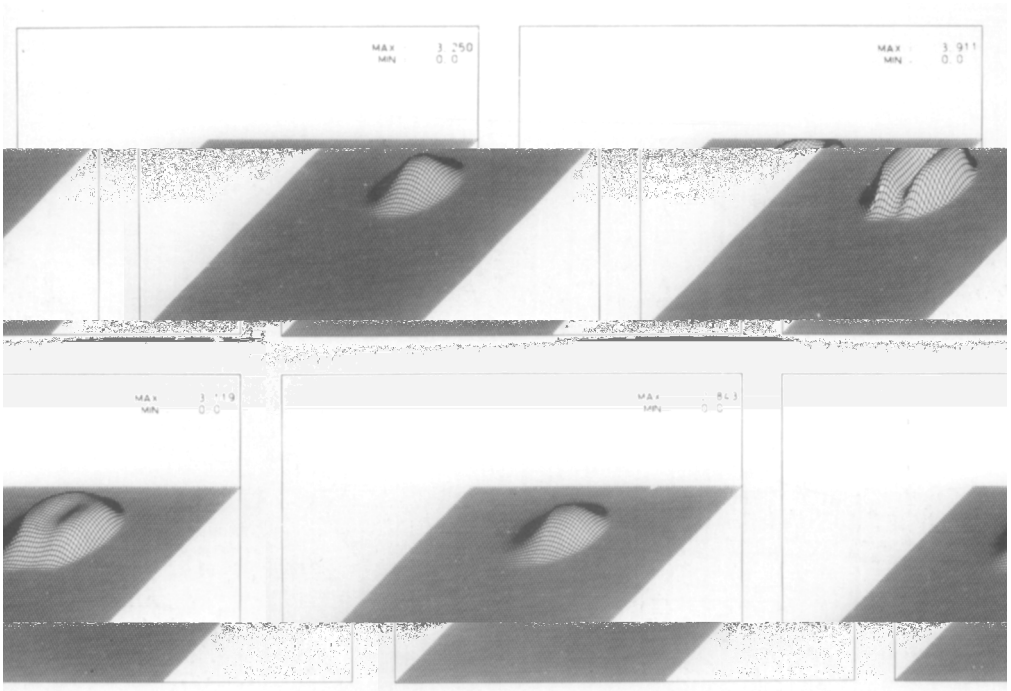

FIG 12. Scheme based on the slope (18)–(20) with $\theta = -1$, $l = 2$.

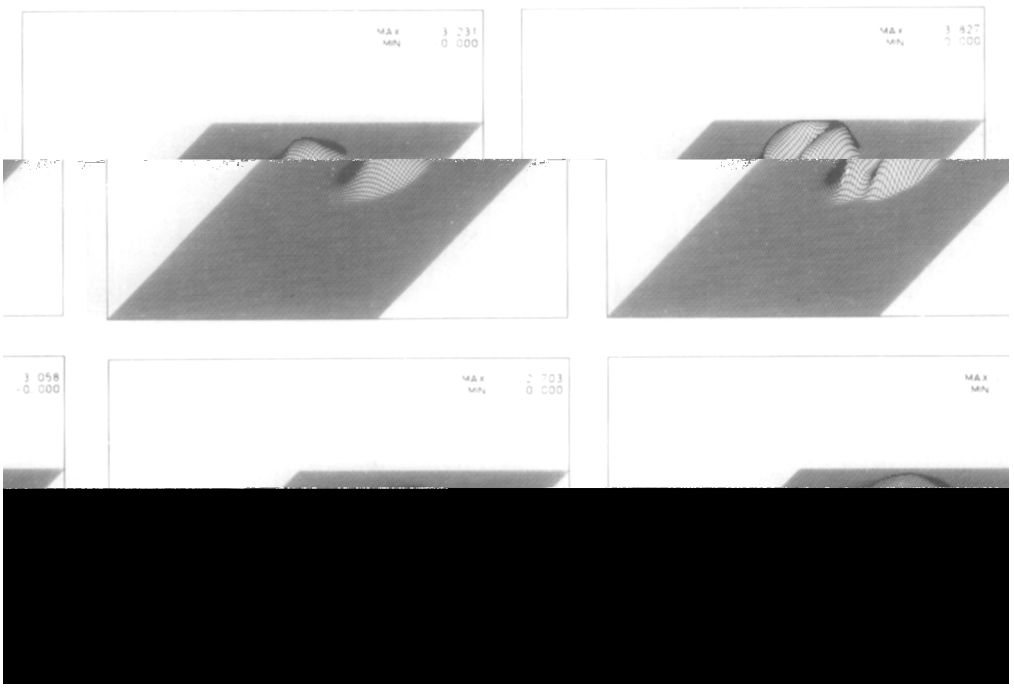

FIG. 13. Scheme based on the slope (21) s_{VA}.

Recently Harten and Osher [12] (see also [3]) have introduced a new class of schemes which they called UNO-schemes (uniformly non-oscillatory). These schemes are required not to diminish the total variation but only the number of local extrema and are allowed occasionally to accentuate a local extremum. They do not possess the clipping phenomena. We used in our calculations the slope proposed in [12] which is a second-order approximation of u_x. It is given by

$$(s_{\mathrm{UNO}})_i = \mathrm{minmod}\left(a_i - \frac{\Delta x}{2} d_{i+1/2}, b_i + \frac{\Delta x}{2} d_{i-1/2}\right), \tag{22}$$

where d denotes the second-order terms

$$d_{i+1/2} = \frac{1}{\Delta x^2} \mathrm{minmod}(u_{i+1} - 2u_i + u_{i-1}, u_{i+2} - 2u_{i+1} + u_i) \tag{23}$$

and a_i, b_i are the first terms given by (11). This UNO-scheme yields the best results for the problem of the rotating cone (see Fig. 14). The form of the cone is preserved very well; after one rotation the maximum of the approximation is less than that of the "superbee cone," but the UNO-scheme does not indicate any clipping. The value of the extremum did not monotonously decrease, but sometimes increased.

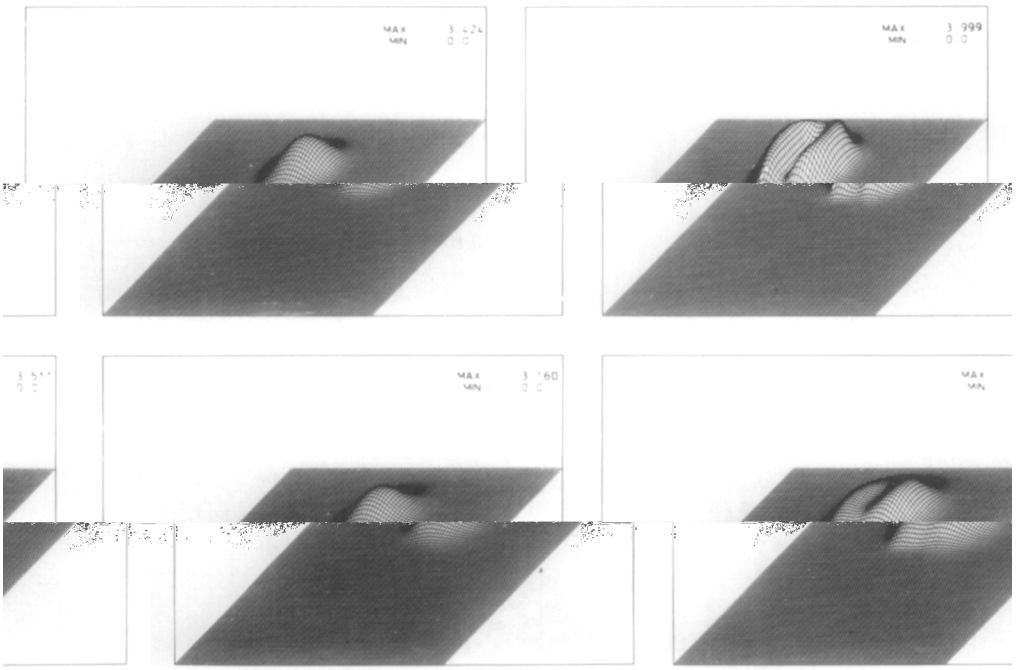

FIG. 14. Scheme based on the slope (22), (23) s_{UNO}.

This effect was limited to the second decimal point in our calculations. The results for the cut-out cylinder are not as perfect as those for the cone. After one rotation the maximal value is greater than that of the scheme using superbee s_2, but the shape is worse. This problem also shows that the UNO-scheme may not preserve the symmetry. We have tried to pick out the best of both schemes—the good approximation of the cone by the UNO-scheme and the good approximation of the cylinder by the superbee—and combined both schemes by hybridization. We used the TVD-scheme for strong gradients and near extrema we switched to the UNO-scheme. But we did not succeed in capturing all desirable features. Although we obtained the best maximum values for both problems and the best resolution of the cut-out cylinder, the results for the cone still indicate strong clipping (see Fig. 15).

There are still some other approaches to obtain a high resolution scheme. Harten [10] in his approach applied a first-order upwind scheme to the conservation law with a modified flux. The added antidiffusive term is chosen in a way that the resulting scheme is a second-order TVD scheme for the original conservation law. For the linear case the scheme of Harten agreed with a MUSCL-type scheme based on the slope s_1 of the class (10). Another way has been given by Davis [8]. He showed that the schemes using flux limiters may also be written as the Lax–Wendroff scheme with an upwind biased artificial viscosity term. Davis [8] succeeded in removing this upwind weighting and obtained a "simple" viscosity

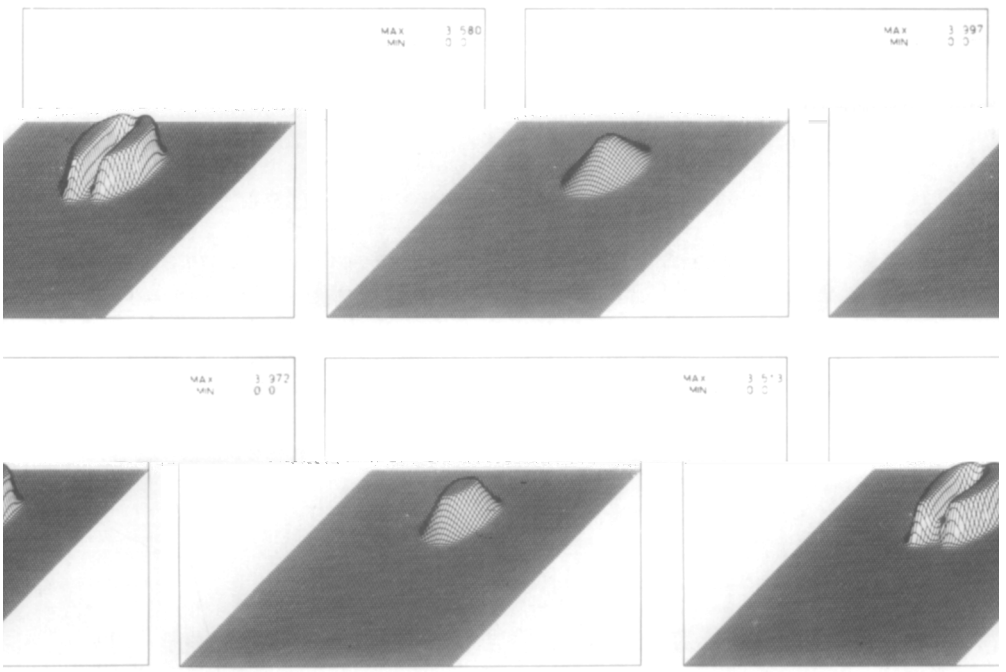

FIG. 15. Scheme based on a hybrid slope of s_{UNO}, s_2.

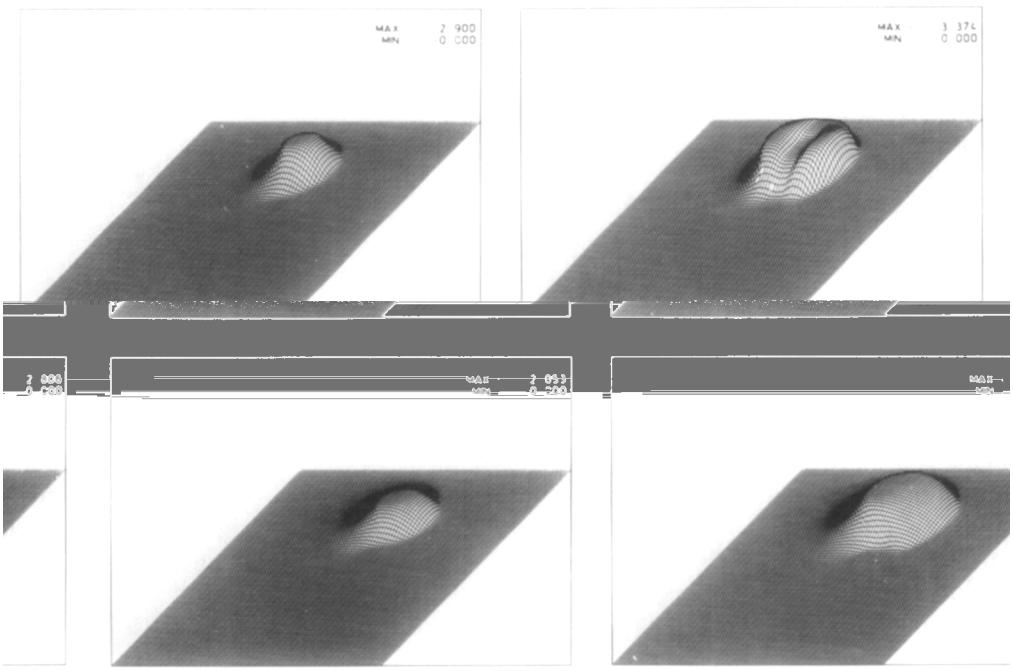

FIG. 16. Symmetric TVD-scheme [8].

term which depends on the ratio of the gradients and which can be added to classical second-order schemes to become TVD. Because these schemes are no longer based on upwind differencing, they are also called symmetric TVD-schemes (see [29]). The results of Davis' TVD-scheme are shown in Fig. 16. It indicates a lack of symmetry.

We will not give exact values of the computer time the different schemes consumed, because we did not optimize in efficiency, and hence these values will give wrong information. We can roughly compare the computational effort in the following way. The Lax–Wendroff scheme consumes more than twice the time required for the Courant–Isaacs–Rees scheme and the high resolution schemes consume about threefold or fourfold time, depending on the computational effort spent to calculate the slopes. For theoretical results about difference schemes for conservation laws see [9, 20, 21] and the references cited here.

4. CONCLUSIONS AND REMARKS

The numerical results for the two initial value problems of Section 2 lead to the following conclusions.

All high resolution schemes considered here reduced very effectively the

numerical dissipation of the underlying low order upwind scheme. The best resolution of discontinuities was achieved by a high resolution scheme based on the "superbee" slope proposed by Roe [24]. It produced excellent results for the test problem with the rotating cut-out cylinder. But the problem with the rotating cone shows a very strong clipping phenomenon of this TVD-scheme. The top of the cone is strongly damped and clipped after a short time. Furthermore, these results show that this scheme is slightly over-compressive and starts to compress the monotone transitions into discontinuities (Figs. 6, 17). For this problem with the cone excellent results have been produced by a UNO-scheme of Harten and Osher [12]. After six rotations the maximum value of the approximated cone is less than that given by the superbee scheme, but the UNO-scheme preserves the shape of the cone much better (Figs. 14, 19). The cut-out cylinder was damped more strongly by the UNO-scheme. The other schemes considered here at not as compressive as that based on the superbee slope, but also the clipping phenomenon is not so visible. The numerical results show that condition (16) for the slopes plays an important role in maintaining symmetry properties of the solution.

Our results for the linear two-dimensional problems give good insight into the behavior of the different high resolution schemes approximating linear and nonlinear discontinuities. For nonlinear problems an over-compressive behavior of a scheme may additionaly cause difficulties at centered rarefaction waves. The monotone transition is compressed into a non-physical discontinuity which is usually called "rarefaction or expansion shock" and which violates the entropy

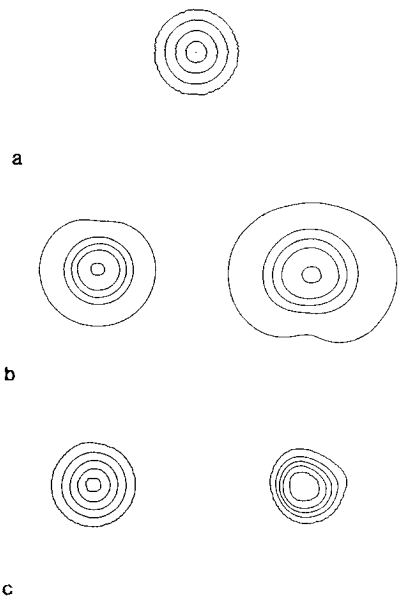

FIG. 17. Contour lines of the exact solution (a) and of the numerical solutions for the rotating cone problem after 1 and 6 rotations (left, right, respectively); (b) Fig. 5; (c) Fig. 6.

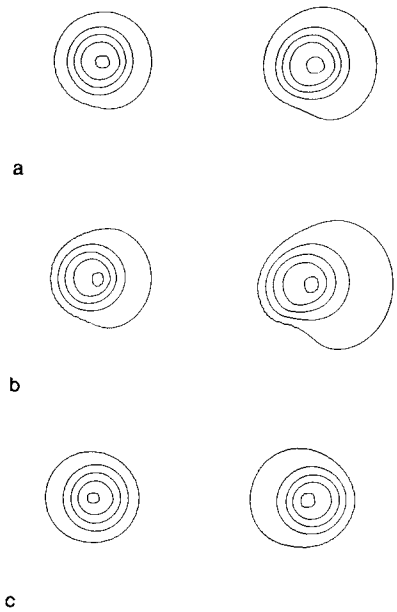

FIG. 18. Contour lines of the numerical solutions for the rotating cone problem after 1 and 6 rotations (left, right, respectively); (a) Fig. 7; (b) Fig. 8; (c) Fig. 10.

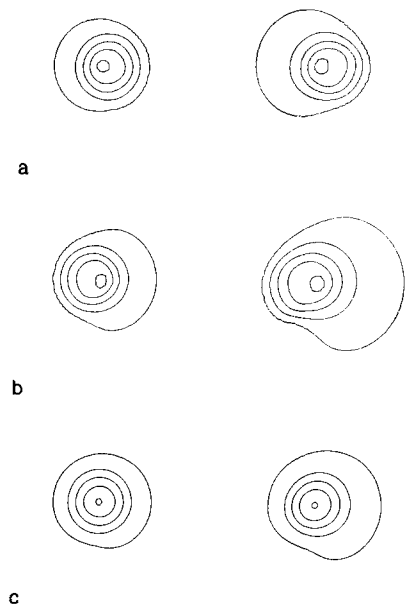

FIG. 19. Contour lines of the numerical solutions for the rotating cone problem after 1 and 6 rotations (left, right, respectively); (a) Fig. 11; (b) Fig. 12; (c) Fig. 14.

condition. These effects are observed in the case of the one-dimensional equations of compressible gas dynamics, the Euler equations, e.g., in [18, 27]. Here the scalar schemes are extended to the system via Roe's [23] or Huang's [13] formal extension. Both are based on a local linearization of the nonlinear system which defines a local system of characteristic fields. The scalar schemes are then applied scalarly to each characteristic field (see also [10]). For the Euler equations these fields are either genuinely non-linear or linearly degenerate. The waves of a linearly degenerate field are exclusively contact discontinuities while the waves of a genuinely nonlinear field are either shock waves or rarefaction waves. Hence, for the linearly degenerate field our results can be applied directly. For the nonlinear fields the superbee slope s_2 may be too compressive at sonic points and may produce rarefaction shocks (see [18, 27]). Thus, for the nonlinear field it is better to use a less compressive slope, e.g., s_{VL}, s_{VA}, s_{UNO}, or $s_{1.5}$, or to switch to a less compressive one near the critical points. Also artificial compression, which may be added to all schemes as a separate step to steepen the discontinuities, should not be applied to centered rarefaction waves. For nonlinear problems there may be different upwind schemes of first-order accuracy and the choice of the upwind scheme within the high resolution algorithm will also influence the numerical results. Some calculations for the Euler equations using different upwind schemes are given in [1, 18]. For simple one-dimensional problems the results turned out to be quite similar [18].

REFERENCES

1. G. D. VON ALBADA, B. VAN LEER, AND W. W. ROBERTS, JR., *Astron. Astrophys.* **108**, 76 (1982).
2. J. P. BORIS AND D. L. BOOK, *J. Comput. Phys.* **11**, 38 (1973).
3. S. R. CHAKRAVARTHY, A. HARTEN, AND S. OSHER, AIAA Paper 86-0330, 1986 (unpublished).
4. S. R. CHAKRAVARTHY AND S. OSHER, AIAA Paper 85-0363, 1985 (unpublished).
5. P. COLELLA AND P. WOODWARD, *J. Comput. Phys.* **54**, 174 (1984).
6. R. COURANT, E. ISAACSON, AND M. REES, *Comm. Pure Appl. Math.* **5**, 243 (1952).
7. M. CRANDALL AND A. MAJDA, *Numer. Math.* **34**, 285 (1980).
8. S. DAVIS, ICASE Report 84-20, 1984 (unpublished).
9. A. HARTEN, *SIAM J. Numer. Anal.* **21**, 1 (1984).
10. A. HARTEN, *J. Comput. Phys.* **49**, 357 (1983).
11. A. HARTEN, *Comm. Pure Appl. Math.* **30**, 611 (1977).
12. A. HARTEN AND S. OSHER, *SIAM J. Numer. Anal.* **24**, 279 (1987).
13. L. C. HUANG, *J. Comput. Phys.* **42**, 195 (1981).
14. P. LAX AND B. WENDROFF, *Comm. Pure Appl. Math.* **13**, 217 (1960).
15. B. VAN LEER, *SIAM J. Sci. Statist. Comput.* **5**, 1 (1984).
16. B. VAN LEER, *J. Comput. Phys.* **32**, 101 (1979).
17. B. VAN LEER, *J. Comput. Phys.* **14**, 361 (1974).
18. C.-D. MUNZ, "On the Construction and Comparison of Two-Step Schemes for the Euler Equations," in *Finite Approximations in Fluid Mechanics*, edited by E. D. Hirschel (Vieweg, Braunschweig/Wiesbaden, 1986), p. 195.
19. S. OSHER, *SIAM J. Numer. Anal.* **22**, 947 (1985).
20. S. OSHER, *SIAM J. Numer. Anal.* **21**, 217 (1984).

21. S. OSHER AND S. CHAKRAVARTHY, *SIAM J. Numer. Anal.* **21**, 955 (1984).
22. P. L. ROE, "Some Contributions to the Modelling of Discontinuous Flows," in *Lectures in Applied Mathematics 22, part 2*, edited by B. Engquist *et al.* (Amer. Math. Soc, Providence, RI, 1985), p. 163.
23. P. L. ROE, *J. Comput. Phys.* **43**, 357 (1981).
24. P. L. ROE AND M. J. BAINES, in *Proceedings, 4th GAMM-Conference on Numerical Methods in Fluid Mechanics*, edited by H. Vivian (Vieweg, Braunschweig/Wiesbaden, 1982), p. 281.
25. P. K. SMOLARKIEWICZ, *J. Comput. Phys.* **54**, 335 (1984).
26. G. STRANG, *SIAM J. Numer. Anal.* **5**, 506 (1968).
27. P. K. SWEBY, *SIAM J. Numer. Anal.* **21**, 995 (1984).
28. P. WOODWARD AND P. COLELLA, *J. Comput. Phys.* **54**, 115 (1984).
29. H. C. YEE, in *Proceedings, Sixth GAMM-Conference on Numerical Methods in Fluid Mechanics*, edited by D. Rues *et al.* (Vieweg, Braunschweig/Wiesbaden, 1986), p. 210.
30. S. T. ZALESAK, *J. Comput. Phys.* **31**, 335 (1979).